The effect of surface finish on the proper functioning of underplatform dampers

Journal of Vibration and Acoustics. Received August 19, 2019;
Accepted manuscript posted January 17, 2020. doi:10.1115/1.4046954

The effect of surface finish on the proper functioning of underplatform dampers

Chiara Gastaldi
Assistant Professor
AERMEC Laboratory
Department of Mechanical
and Aerospace Engineering
Politecnico di Torino
Torino, Italy, 10129
Email: chiara.gastaldi@polito.it

Teresa M. Berruti
Associate Professor
AERMEC Laboratory
Department of Mechanical
and Aerospace Engineering
Politecnico di Torino
Torino, Italy, 10129
Email: teresa.berruti@polito.it

Muzio M. Gola
Professor Emeritus
AERMEC Laboratory
Department of Mechanical and Aerospace Engineering
Politecnico di Torino
Torino, Italy, 10129
Email: muzio.gola@polito.it

ABSTRACT

Underplatform dampers are used to limit the resonant vibration of turbine blades. In recent years, various strategies have been implemented to maximize their damping capability. Curved-flat dampers are preferred to ensure a predictable bilateral contact, while a pre-optimization procedure was developed to exclude all those cross-sectional shapes that will bring the damper to roll and thus limit the amount of dissipated energy. The pre-optimization bases its predictions on the assumption that the effective width of the flat contact interface corresponds to the nominal one. It is shown here that this hypothesis cannot be relied upon: the energy dissipated by two nominally identical dampers, machined according to the usual industrial standards, may differ by a factor up to three due to the morphology of the flat-to-flat contact interface.Five dampers have been tested on two dedicated test rigs, available in the AERMEC laboratory, specially designed to reveal the details of the damper behavior during operation.. Their contact interfaces are scanned by means of a profilometer. In each case, the mechanics, the kinematics and the effectiveness of the dampers in terms of cycle shape and dissipated energy are correlated to the morphology of the specific contact surface. To complete the picture, a state-of-the-art numerical simulation tool is used to show how this tribo-mechanic phenomenon, in turn, influences the damper effect on the dynamic response of the turbine.

1 Introduction

In the last decades underplatform dampers for turbine blades have been the subject of in-depth studies both from the point of view of modeling [1–6] and design [7–10].

Contact modeling is certainly one of the most critical points. In fact, a commonly shared strategy is not yet present, as demonstrated by the wide range of models proposed over the last few years [11–17]. One of the most common modeling choice for conforming contacts is to apply node-to-node 2D [11] or 3D [18, 19] contact elements. In some cases, the contact surface is discretized in a high number of nodes, i.e. the so called "high-fidelity" modeling [5, 10, 20]. This choice allows to

mimic, even if not in an optimal way, the microslip (gradual sliding of mating surfaces). Other authors prefer instead to minimize the number of contact elements since it was demonstrated that a good experimental-numerical match of kinematic and force related quantities can be obtained provided that the position of the contact force resultant is accurately reproduced [21]. Some general assumptions are common to both modeling strategies. Namely, the width and length of the effective contact interface is generally assumed to correspond to the nominal one (for lack of a better assumption). Furthermore, it is usually assumed that all contact elements share the same contact parameters (i.e. uniform distribution). These assumptions, however convenient, must be improved with the help of additional tribological information if one wishes to obtain a successful experimental-numerical comparison [22].

The extensive experimental evidence gathered by the authors in recent years confirms the need for improvement whenever conforming contacts are to be simulated. The problem becomes even more pressing if one considers that the same assumptions used for simulation (e.g. nominal contact area) are also used at the design stage. It will be shown here that five nominally identical damper samples, whose configuration has been selected using the pre-optimization procedure [9], give origin to markedly different damping contributions.

Section 2 will present the AERMEC experimental and modeling capabilities using a "lucky" measurement prototype characterized by a fairly uniform flat-on-flat contact. In this fortunate, although rare case, the damping efficiency is high, contact parameters can be easily estimated using the in-house procedure, and the damper mechanics and kinematics can be effectively simulated using a standard numerical model.

Section 3 demonstrates how a non-uniform flat-on-flat contact makes the procedure for estimating contact parameters inapplicable and the standard damper numerical model inadequate.

Section 4 demonstrates how a non-uniform flat-on-flat contact can reduce by a factor of three the damping efficiency. Nevertheless the tribo-mechanical experimental evidence available to the authors provides a full understanding of the dampers behaviour and their connection to the specific contact conditions.

Section 5 exploits the complete tribo-mechanical understanding of the behavior of the flat-on-flat surfaces to build simple but effective numerical models capable of representing the different non-uniform contacts encountered during the present analysis.

Section 6 propagates the tribo-mechanical sample-to-sample variability to the dynamic response of a bladed disk coupled by underplatform dampers.

2 Methodology

Five samples are assessed within this work. Each sample is composed of one damper and two platform inserts. All samples share the same dimension, shape, platform angles and have been obtained using the same machining procedure. Further details on the samples material and testing conditions can be found in Table 1. In detail the centrifugal load affects the contact parameter values, while the excitation frequency does not influence neither the contact parameters nor the damper performance [23]. Additional information on the machining process can be found in Sect. 2.1. All samples are tested on a Piezo Damper Rig, a testing facility designed, built and assembled by the AERMEC laboratory to the purpose of

– measuring the in-plane forces transferred between the blade platforms through the under-platform damper as consequence of their relative displacements (i.e. underplatform damper mechanics);
– provide an estimate for the contact parameters necessary to numerically simulate their effect on turbine blades.

The first version of the test rig was developed in 2009 [24] and has been used to test samples 1 and 2. The frequency and centrifugal load limitations (see Table 1) of the rig have been overcome by its second version, developed in 2016 [25] and shown in Fig. 2-1a[1]. Both rigs share the same architecture, i.e. two distinct parts, each one representing a platform (i.e. hosting one platform insert). The right one is static and accommodates the load cells, which measure the forces in two perpendicular directions; the left part produces the in-plane motion, actuated by piezoelectric stacks. This paper focuses on blade in-phase motion, as this is the closest condition to the in-service reference cases known to the authors. In-phase vibration translates into vertical relative platform motion, as demonstrated by the functional scheme shown in Fig. 2. The test rigs focus on all in-plane platform displacements [23], as blade bending modes are typically encountered at lower frequencies and characterized by larger amplitudes. The investigation of out of plane vibration would require a different experimental set-up. A laser head is used to record the relative platform motion[2], the relative platform-damper motion at the contact interfaces and the damper rotation. Section 2.2 presents a sample of results taken from Sample 1.

2.1 Machining process and the effect of wear

The curved-flat dampers from Samples 3 to 5 are obtained from real dampers typically mounted on the fourth stage of a gas turbine for energy production. Similarly, the corresponding platform inserts are obtained from the platforms of one blade of the above-mentioned turbine. A series of machining operations have been performed to adapt the dampers and platform inserts to the rig:

– reducing the axial length of the damper to fit the rig;
– drilling four holes on the damper (close to its center of mass) to allow for the centrifugal load application, here simulated by a series of deadweights;
– machining a series of cuts on the upper part of the damper (away from the contact areas) to necessary to kinematic measurements (see Fig. 3d and Sect. 2.2);
– removing a portion of platform to host the head of the screws used to connect the insert to the rig, thus leaving two 4 mm wide protrusions which serve the double purpose of localizing the contact along the damper axis and increasing the contact pressure (see also Fig. 1b).

None of the above mentioned machining operations modifies the contact surfaces of damper and platform inserts.
Dampers and platform inserts from Samples 1 and 2 are obtained from regular steel by an in-house workshop, however the finishing and roughness specifications of the contact surfaces match those of Samples 3 to 5.
Results shown here refer to dampers which have undergone a run-in process, i.e. $> 7 \cdot 10^6$ cycles before measurement.

[1]For this reason a direct comparison of Samples 1-2 and 3-4-5 is not possible (different experimental boundary conditions).
[2]The authors are using a differential laser to measure the $w_{LP} - w_{RP}$ signal as shown in Fig. 3 because in the first version of the test rig the sub-optimal stiffness of the force measuring block allowed for small movements (≈ 0.5 μm) of the right platform. This has become unnecessary in the second version of the test rig, where the right platform is truly "static".

This corresponds to a mean value of total dissipated energy at the flat-on-flat contact of 6200 J (i.e. approximately 0.89 mJ per cycle) which is in accordance with recent results on flat-on-flat contacts [26] which set the limit to reach steady state at 3000 J and $2.1 \cdot 10^6$ cycles. Furthermore, it was observed in [23] that dampers' performance and contact parameters show a larger variability if measured during the initial tests but reach stable and repeatable values within 5-6 million cycles (all recorded values after this point lie scattered within the uncertainty bands). It should be stressed that after the initial changes observed during the run-in process (which also produce visible wear traces on the damper surface) no subsequent evolution and relevant change in the dampers' performance and/or contact parameters have been observed during the experimental campaign ($[1-2] \cdot 10^9$ cycles). The lack of effects of wear will be further commented on in Sect. 4.

2.2 A measurement prototype

The purpose of this section is to present the experimental evidence made available by the Piezo Damper Rigs and the basics of contact parameter estimation. All measured and derived quantities described here come with a confidence interval (in all cases $< 5\%$). A full description of the measurement error estimation technique can be found in [27]. Sample 1 has been purposely chosen as a demonstrator: the morphology of its flat-on-flat contact interface, as will be pointed out in Sect. 2.3, allows for the contact parameter estimation procedure to be successfully and completely carried out.

Platform-to-platform hysteresis cycle The diagram that best represents the overall damper performance is the Platform-to-platform hysteresis cycle. The relevant quantities recorded in case of IP motion are shown in Fig. 3a. The platform-to-platform hysteresis diagram is capable of summarizing the effect of the damper between the blades, both in terms of stiffening and of damping effect. The x axis of the diagram in Fig. 3b shows the relative platform motion over one period of vibration (measured by means of a differential laser head). In case of pure In Phase (IP) blade vibration this motion is purely vertical. The y axis of the diagram shows the component of one of the contact forces (either left or right) aligned with the relative platform displacement during one period of vibration. In the IP case the relevant force component is the vertical one, here termed V_R (the right component is here preferred as it is directly measured by the load cells). The platform-to-platform hysteresis cycle is quite representative of the damping effect. In fact, the area inside the hysteresis curve represents the global dissipated energy. Since the imposed motion is quite large (i.e. $> \pm 20$ μm), the dampers are expected to reach the gross slip condition and therefore to dissipate energy. The area of the cycles is compared to that of an ideal rectangle, represented using dashed grey lines. Its sides are as large as the maximum excursion of V_R and as large as the imposed platform motion. This ideal rectangle represents the area the cycle would have if the contact stiffness $- >$ inf and if the damper behaved following a regular stick-slip pattern. The ratio between the actual area of the cycle and its ideal counterpart is defined as "damping efficiency", the corresponding values for the five Samples investigated within this work can be found in Table 1. The shape of the cycle in Fig. 3b is regular, typical of a highly efficient stick-slip pattern, thus confirming the prediction of the pre-optimization maps (i.e. the configuration of the dampers here tested has been chosen inside the design area).

The damper static equilibrium The flat-on-flat contact force resultant and its position are derived using the damper equilibrium of forces and moments shown in Fig. 3c. This procedure neglects the damper inertia forces which were proven

to be negligible for excitation frequencies lower than 50 kHz [27]. The left contact force resultant is used in a series of diagrams outlined below

Platform-to-damper hysteresis cycles The platform-to-damper hysteresis cycles plot the relative displacement at the contact against the corresponding tangential component of the contact force. The relative displacement at the contact is obtained by pointing the laser as described in Fig. 3d. The force is either directly measured (T_R) or obtained through the damper static equilibrium mentioned above (T_L). The platform-to-damper hysteresis cycles are used to estimate tangential contact stiffness values (see paragraph below).

Tangential over normal force ratio The ratio between the tangential and normal force components at the (left and right) contact interfaces can be plotted as a function of time as in Fig. 3f. The diagram allows to divide the period of vibration into portions, each signaled by colored markers visible on the diagrams in Fig. 3 and characterized by a specific contact state. When the T/N ratio is constant in time and equal to a maximum, then the corresponding interface is in gross slip condition and the T/N value may be interpreted as a friction coefficient. When the T/N ratio is varying with time, then the contact state is stick and the corresponding stage on the platform-to-damper hysteresis cycle can be used to estimate the tangential contact stiffness.

Contact forces diagram Contact forces can be represented as vectors on the damper surface, as shown in Fig. 4a. In detail, the left contact force resultant travels along the flat damper-platform surface during the cycle. The position of the left contact force resultant has important consequences on the overall damper performance. Should the left contact force resultant F_L reach one of the edges of the flat contact surface, that edge will serve as a hinge and the damper will roll (a state known as lift-off), leading to a large damper rotation. Lift-off is very detrimental for the damping efficiency as demonstrated in previous works [9], and makes contact parameter estimation difficult.

Moment vs. rotation diagram Getting a true estimate of normal contact stiffness is a challenging task. While for cylinder-on-flat interfaces, analytical models are available in the literature [28], no widely recognized guidelines are available for flat-on-flat interfaces. The task is made even more complicated by the fact that the damper-platform flat-on-flat interface is loaded by a force resultant that varies both in amplitude and in position during the vibration cycle. An ad-hoc technique is therefore necessary.

The key idea behind the technique shown here is to link the damper inclination (i.e. rotation angle β_D[3] at a given instant in time) to the position of the left contact force resultant N_L (i.e. moment M of N_L around point O in Fig. 4b). In other words, it is postulated that forces (i.e. moments) and displacements (i.e. rotation) are linearly linked. The technique also relies on two assumptions:

1. the normal contact stiffness is uniformly distributed along the flat interface;

[3]measured by pointing the differential laser head as shown in Fig. 1a and dividing the resulting signal by the distance between the laser pointers as described in [21]

2. the force per unit length $q(x)$ related to the normal component of the left contact force resultant N_L has a linear distribution.

For each instant in time it is possible to determine, under the assumptions above, which portion of the flat interface is actually in contact. If N_L enters the inner third portion of the flat interface, as shown in Fig. 4c, the complete surface is in contact. In that condition, the normal contact stiffness per unit-length can be expressed as:

$$\frac{dk_{nL}}{dx} = \frac{12M}{\beta_D L^3} \tag{1}$$

where L is the length of the flat contact surface (segment $\overline{AB}$ in Fig. 4a). Further details on the derivation of Eq. 1 can be found in [27]. The validity of the model assumed to represent the normal force-normal approach relation is confirmed by the experimental evidence shown in Fig. 4d. The slope of the moment vs. rotation diagram keeps constant whenever N_L falls within the inner third portion of the contact interface.

2.3 Modeling capabilities

The contact parameter estimation technique described in Section 2.2 has had full success on Sample 1. The contact parameters thus obtained are fed to a numerical simulation tool of the damper-platform system [9] shown in Fig. 5a. The damper is modeled as an in-plane rigid body connected to two platforms with assigned motion by means of a 2D contact element [2]. The damper equilibrium equations are solved using an in-house time marching technique [29]. The resulting experimental-numerical comparison is fully congruent as shown in Fig. 3-4. The successful modeling effort is partly due to the configuration of the flat-on-flat contact interface. Both platform and damper surfaces have been scanned by means of a profilometer.

A total of six scanning lines are taken from each of the contact surfaces, as shown in Fig. 1b. The resulting profiles are remarkably repeatable, see Fig. 5b for two examples from the damper contact surface. The repeatability is mainly due to the trajectory followed by the tools during the machining process.

The damper and platform profiles can then be combined to visually reproduce the contact status, as shown in Fig. 5c. The relative transverse position of the two surfaces (i.e. alignment along x axis in Fig. 5) is known with an uncertainty of 0.1 mm, obtained through photographic documentation of the experimental set-up and confirmed by the wear traces. It can be seen that, while the surfaces are far from actually flat, asperities from the two surfaces come into contact at uniform intervals across the contact length. As shown above, this uniformly distributed contact can be modeled using only two contact elements (as in Fig. 5a) sharing the same parameters (k_{tL},k_{nL} and μ_L).

The conformation of the flat-on-flat contact surface of Sample 1 is only one of those possible and, in the experience of the authors, it is not often encountered. The following Sections deal with the remaining samples from Table 1, showing how different configuration of the flat-on-flat contact surface can affect the damper performance and the capability to estimate contact parameters and reproduce numerically the damper behaviour.

3 Sample 2: how a non-uniform flat-on-flat contact interface can impair the capability of estimating contact parameters

Sample 2 is a nominally identical to Sample 1. It was produced using the same machining procedure, machining tools and material. Nevertheless, the resulting Moment vs. Rotation diagram, shown in Fig. 6b, is markedly different with respect to the one obtained from Sample 1. The reader will notice that the classical S shape seen in Fig. 4b is not present in Fig. 6a. There is still linearity between the moment M and the rotation β_D in given portions of the cycle. However, around M=0 N/mm^2, the rotation is not matched by a corresponding moment variation (i.e. stages 2-3 and 6-7 in Fig. 6a-b), even though the contact force resultant lays in the innermost portion of the flat-on-flat interface (points 2-3 and 6-7 in Fig. 6a). This behaviour is repeatable and observed at different CF values on the damper, here not shown for brevity.

The reason behind this seemingly strange behaviour is found by observing the contact surface mating profiles. In the case of Sample 1, the contact is ensured by uniformly distributed discrete clusters of mating asperities sharing $\approx$ the same height. The platform from Sample 2, on the other hand, sports two central "bumps" (i.e. "clusters" of asperities whose mean height is larger than the surrounding ones), named pivots 2-3 and 6-7 in Fig. 6c. As a result, when $\beta_D \approx 0$ and the force F_L is close to one of these pivot points, the edges of the damper will not be in contact, leaving the damper "free" to rotate. As the damper continues its rotation, "pushed" by the platform kinematics, the moment will remain $\approx$ constant until the contact at one of the outer edges has not been regained.

It is worth noting that it was possible to obtain a complete explanation of the phenomenon only thanks to the combination of experimental evidence of various types: kinematics and contact forces from the test rig and profile configuration from the profilometer. The sub-optimal flat-on-flat interface configuration has a number of consequences both on the damper performance and on the operator's ability to simulate its beahviour.

- The damper efficiency decreases, as demonstrated by the comparison between the platform-to-platform hysteresis cycles from Sample 1 and 2 in Fig. 7a. The cycle corresponding to Sample 2 sports two discontinuities caused by the left contact force resultant passing across the "pivot points". This causes the damping efficiency, here defined as the area of the cycle over the area of the corresponding "ideal cycle", to drop from 80% (Sample 1) to 71% (Sample 2).
- The uniform distribution of normal contact springs postulated in Sect. 2.2 and used to estimate k_{nL} is not valid if Sample 2 is considered. This makes it hard both to provide an estimate for k_{nL} and impossible to simulate its moment-rotation relation with the simple model shown in Fig. 5a
- The platform-to-damper hysteresis at the flat-on-flat interface is also affected. While the cycle corresponding to Sample 1 (see Fig. 3e) displays a unique slope during full stick, Sample 2 sports a "double-slope", as shown in Fig. 7b. The initial portion of the full stick state (black markers) corresponds to a portion of the cycle where rotation is minimal and F_L is away from the pivots area (see Fig.7c). When F_L moves across the pivots area, the contact state is still full-stick[4]. However the slope of the platform-to-damper hysteresis cycle (red markers in Fig. 7b) decreases dramatically. This may be partially due to the local conditions of the portion of surface in contact. However the increased rotation signal may have polluted the relative displacement laser signal, as described in [25]. Once again the model with uniform contact

[4]The full stick state is confirmed by the T/N ratio diagram, here not shown for brevity.

parameters in Fig. 5a is not adequate and a unique estimate for k_{tL} cannot be provided.

4 Samples 3, 4 and 5: how a non uniform contact surface can strongly affect the damper efficiency

This section deals with Samples 3,4 and 5, obtained from real-life dampers and blade platforms. The three dampers share the same configuration as Samples 1 and 2 (i.e. platform angles and damper cross-section shape). Since the dampers' configuration is "pre-optimized", the resulting platform-to-platform hysteresis cycles are expected to be highly efficient (i.e. area close to that of the corresponding ideal cycle) and to display a regular Coulomb-like shape. The platform-to-platform hysteresis cycles obtained under the same nominal experimental conditions from Samples 3,4 and 5 are shown in Fig. 8. The shape of the cycles is consistent for different values of centrifugal loads on the dampers, here not shown for brevity. The shape and area of cycles 3 and 4 are far from ideal: their banana-like shape is typically connected to damper rolling, as will be confirmed by the large rotation signals.

Once again, it is deemed necessary to combine the experimental evidence from the test rig with the profilometer's output.

4.1 Sample 3

The contact surface of the platform insert is composed of two different planar surfaces with different inclinations. As shown in Fig. 9, the two inclinations are present in both tracks of the insert[5]. Since the asperities on the damper surface have a uniform height (here not shown for brevity), the double inclination of the insert surface seems to be the main cause of the damper rotation. This is confirmed by contact forces diagram in Fig. 10a, compared with the measured rotation of the damper in Fig. 10b: the damper stops rolling exactly when the left contact force resultant falls on the upper platform surface (red line in Fig. 9 and points 4-5-6 in Fig. 10a). Furthermore the 10 mrad relative inclination of the two surfaces of the platform insert is perfectly compatible with the >5 mrad damper rotation.

4.2 Sample 4

The area of cycle 4 is larger than that of cycle 3, however its "banana" shape denunciates a non negligible damper rotation. Once again, the profilometer results combined with the contact forces diagram and damper rotation give a full explanation of the damper behaviour. Figure 11a shows how the assumption that the nominal flat-on-flat contact surface corresponds to the actual one is not valid in this case.

While the roughness limits are acceptable, it is the lack of planarity which strongly influences the damper behaviour. The contact on the right portion of the surface is ensured (2.6 mm long segment in Fig. 11a-b). This is in perfect agreement with the experimental evidence from Fig. 11c: when the left contact force resultant falls in that region (points 3-4-5) the damper does not roll. On the contrary, when the contact force resultant falls on the left portion of the contact surface (stages 1 to 2 and 5 to 1), where the mating of the two surfaces is far from optimal, the damper starts rolling. In detail there is an evident peak on the damper surface, 1.7 mm away from the "nominal" left edge, which clearly serves as a hinge (in fact the left contact force resultant stops 1.7 mm away from the edge, point 1 and 6 in Fig. 11b). Furthermore the lack of material on the

[5]The damper profile is here not represented as the effect of its profile is one order of magnitude smaller than the double slope evidenced on the platform.

corresponding portion of the platform lets the damper rotate freely.

4.3 Sample 5

The authors initially hoped that wear and fretting would even out the asperities detected in Fig. 11a. Sample 4 was therefore exposed to a quite lengthy experimental campaign ($> 5 \cdot 10^8$ cycles under realistic nominal contact pressures). Unfortunately, no such beneficial effects were detected. While the authors cannot rule out the possibility that wear will eventually improve contact distribution, they are forced to point out that quite a few cycles may be spent by dampers in sub-optimal conditions due to imperfect flat surface mating. This is why the authors suggest an alternative solution based on machining.

Sample 5 has been obtained from Sample 4. The damper has been purposely re-machined in order to ensure that the contact extends up to the two nominal edges. A 50 μm deep cut was then machined in the central portion of the flat damper surface, as shown in Fig. 12a, thus leaving two 1.5 mm wide outer protrusions where the contact is concentrated. Despite the lack of planarity of the platform insert, left unchanged, the contact force resultant application point is now able to complete its trajectory across the contact surface without reaching its edge (see Fig. 12a). As a consequence, rotation is limited (< 1 mrad) and the damping efficiency is high as shown in the platform-to-platform hysteresis cycle of Fig. 8 and Table 1.

This simple and cost-effective machining operation appears as a robust solution to the inevitable lack of planarity of mating flat surfaces leading to high sample-to-sample variability. While it is true that the nominal contact pressure will increase, this should not impair the damper performance. It is should be stressed that the actual contact pressure experienced by Sample 4 is not much lower that experienced by Sample 5. Simply, in the case of Sample 4 (i.e. nominally flat surface) the user has no control nor prior knowledge over the extension of the true contact area.

If wear were to take place, the presence of the two edges would speed up the process and gradually lead to a truly flat contact surface.

5 Modeling contact surfaces

As stated above, the simple damper numerical model of Fig. 7 is not fit to represent complex contact conditions such as those encountered when analyzing Samples 3 and 4. Nevertheless, modeling non-uniform flat-on-flat contact surfaces is still possible. Figure 13a shows the simulated counterpart of the measured platform-to-platform hysteresis cycles of Fig. 8. The tribo-mechanical experimental evidence recounted in Sect. 4 provides the authors with enough information to modify the model in Fig. 5a. In detail the damper is modeled as a rigid body with three in-plane degrees of freedom at its center of mass. The damper-platform contact is simulated through a series of 2D contact elements [2] with normal and tangential contact stiffness. One element is used to simulate the cylinder-on-flat contact as in Fig. 5a while a total of three appropriately arranged elements are used to represent the flat-on-flat contact surface as shown in Fig. 13b and c for Samples 3 and 4 respectively. The reader will notice that some of the elements are equipped with a gap vector, set at 55 μm and 3.5 μm to mimic the morphology of the surfaces shown in Fig. 9 and 11a respectively. The centrifugal load is applied directly at the damper center of mass and no further assumption is made on the contact surface at the contact. An

alternative approach to represent uneven flat-on-flat contact surfaces without resorting to contact elements with a gap is to apply a pressure distribution, as was done in [22]. The contact parameters used in the simulation of Samples 3 and 4 are tentatively set equal to those estimated on Sample 5 using the contact parameter estimation technique recounted in Sect. 2.2. The ultimate goal is here not to obtain a perfect experimental numerical match, rather to capture the essential characteristics of the hysteresis shape taking advantage of the information on the profile morphology.. In detail, the double slope of the platform insert from Sample 3 is represented using three contact elements whose position has been selected using Fig. 9-10 and equipped purposely tuned gap vectors. Similarly the position of the contact elements in Figure 13c has been selected using the information from Fig. 11. This considerable simulation effort has been taken up by the authors to provide a further proof of the complete understanding of the interaction between tribology and damper mechanics. Furthermore the models thus obtained will be used in Sect. 6 to evaluate the repercussions that a non-uniform flat-on-flat contact interface can have on the dynamics of a bladed disc. Nevertheless it should be stressed that contact conditions such as those encountered in the case of Sample 3 and 4 should be avoided, rather than simulated. Sample 5, in fact, is not only more efficient, but can also be successfully represented using the standard damper numerical model shown in Fig. 5a.

6 From tribo-mechanics to dynamics

The damper numerical models described in Sect. 5 can be used to explore the consequences that different contact conditions have on the dynamics of a bladed disk. A simplified blade is modeled using a commercial FE code and the size of the model is then reduced using CB-CMS [30]. The reduced model is then imported in FRIDA environment, a state-of-the-art in-house nonlinear iterative solver, called "FRIDA" whose complete description can be found in [31, 32]. Once in FRIDA, cyclic symmetric boundary conditions are used to impose an In-Phase mode of vibration (zero nodal diameter)[6] and the blade FE model is coupled to the damper rigid body model by means of contact elements, as shown in Fig. 5a and 13b-c. Harmonic Balance is used to solve the nonlinear equilibrium equations of the blade-damper system. The output is the well known frequency response function (FRF), here taken at a point at the tip of the blade.

Figure 14 shows three FRFs, one for each Sample from Sect. 4-5, obtained using the same forcing level. In addition, the free (i.e. no damper) FRF is partially shown in the figure and here used as a reference. The frequency and amplitude of the free response peak are 351 Hz and 17.4 10^{-4} m/N respectively. While all damper samples lead to a stiffer response (higher resonance frequencies) and to a lower amplitude with respect to the free peak reference, there are also significant differences among the three samples. The comparison between the three dynamic responses confirms the findings from Sect. 5. The curve corresponding to Sample 5 shows the lowest maximum (i.e. higher damping efficiency). The curves corresponding to Samples 3 and 4, on the other hand, display higher levels of displacement and a markedly softening behavior (typical of lift-off and rolling motion).

These curves have been obtained using three different numerical models which, however, correspond to three nominally identical dampers. It is worth noting that the response may double (i.e. curve 3 is twice as high as curve 5) depending on

[6] Both the blade and the engine order excitation chosen here replicate a real condition known to the authors.

the morphology of the flat-on-flat contact interface[7]. It can therefore be concluded that a uniform distribution of contact elements to simulate a flat-on-flat contacts, as already observed in [22], is a dangerous practice as it may lead to a incorrect predictions and an over-estimation of the friction damping contribution.

7 Conclusions

The present experimental-numerical investigation made use of five different damper-platform samples, tribological information coming from a profilometer, two different test rigs for the investigation of the damper mechanics and state-of-the-art simulation capabilities to evaluate the consequences of surface-to-surface variability on the dynamics of a bladed disk. The main conclusions that can be drawn from this experimental-numerical investigation are listed below.

1. Although the platforms and damper samples abide by typical industrial manufacturing and finishing tolerances, the assumption that the extension of nominal and effective flat-on-flat contact surfaces coincide cannot be relied upon.
2. Depending on the morphology of the flat-on-flat interface the damper efficiency may decrease by a factor of three as observed by the authors.
3. Uneven contact surfaces not only diminish the damping capability of the damper, but may also impair contact parameter estimation procedures based upon uniform contact assumptions.
4. The combined tribo-mechanical experimental evidence coming from the profilometer and Piezo Damper Rigs respectively, can explain the sample-to-sample variability and relate it to the specific morphology of the contact surface.
5. The full understanding of the mechanics of the damper, confirmed by tribological information, can help the user build adequate models to represent non-uniform flat-on-flat contacts.
6. The models from point 5 can then be used to evaluate the surface-to-surface variability on the dynamics of a bladed disk. This first set of results obtained on a simplified model confirms the dramatic influence of flat on flat contact surfaces: response curved may vary by a 100 % factor.
7. From a designer's point of view, this variability is unacceptable, as it nullifies any optimization effort. Rather than taking into account this variability, the primary goal should be to minimize it.
8. The collective evidence gathered in this paper demonstrates that current manufacturing and finishing tolerances may not be adequate to ensure the damper proper functioning.
9. A practical and cost-effective alternative is that of removing the central portion of the flat damper contact surface, thus forcing the damper to touch onto two outer protrusions. This solution is effective in ensuring a predictable damper behaviour but may increase the contact pressure.

Acknowledgements

The authors would like to thank Ansaldo Energia for funding the csntruction of the Piezo Test Rig II, used throughout the present experimental investigation

[7]This variability may change if mistuning is taken into consideration, i.e. different dampers having different contact surfaces.

References

[1] Griffin, J., 1980. "Friction damping of resonant stresses in gas turbine engine airfoils". *Journal of Engineering for Power,* ***102***(2), p. 329.

[2] Yang, B. D., and Menq, C. H., 1998. "Characterization of contact kinematics and application to the design of wedge dampers in turbomachinery blading: Part 2—prediction of forced response and experimental verification". *Journal of Engineering for Gas Turbines and Power,* ***120***(2), p. 418.

[3] Ciğeroğlu, E., An, N., and Menq, C., 2007. "Wedge damper modeling and forced response prediction of frictionally constrained blades". In Volume 5: Turbo Expo 2007, ASME.

[4] Petrov, E. P., and Ewins, D. J., 2007. "Advanced modeling of underplatform friction dampers for analysis of bladed disk vibration". *Journal of Turbomachinery,* ***129***(1), p. 143.

[5] Petrov, E., 2008. "Explicit finite element models of friction dampers in forced response analysis of bladed disks". *Journal of Engineering for Gas Turbines and Power,* ***130***(2), p. 022502.

[6] Schwingshackl, C., Petrov, E., and Ewins, D., 2012. "Effects of contact interface parameters on vibration of turbine bladed disks with underplatform dampers". *Journal of Engineering for Gas Turbines and Power,* ***134***(3), p. 032507.

[7] Panning, L., Sextro, W., and Popp, K., 2000. "Optimization of interblade friction damper design". In Volume 4: Manufacturing Materials and Metallurgy Ceramics Structures and Dynamics Controls, Diagnostics and Instrumentation Education, ASME.

[8] Panning, L., Popp, K., Sextro, W., Götting, F., Kayser, A., and Wolter, I., 2004. "Asymmetrical underplatform dampers in gas turbine bladings: Theory and application".

[9] Gastaldi, C., Berruti, T. M., and Gola, M. M., 2018. "Best practices for underplatform damper designers". *Proceedings of the Institution of Mechanical Engineers, Part C: Journal of Mechanical Engineering Science,* ***232***(7), pp. 1221–1235.

[10] Hls, M., von Scheidt, L. P., and Wallaschek, J., 2018. "Influence of geometric design parameters onto vibratory response and HCF safety for turbine blades with friction damper". In Volume 7C: Structures and Dynamics, ASME.

[11] Yang, B., Chu, M., and Menq, C., 1998. "Stick-slip-separation analysis and non-linear stiffness and damping characterization of friction contacts having variable normal load". *Journal of Sound and Vibration,* ***210***(4), mar, pp. 461–481.

[12] Segalman, D. J., 2005. "A fourparameter iwan model for laptype joints". *Journal of Applied Mechanics,* ***72***(5), p. 752760.

[13] Krack, M., Salles, L., and Thouverez, F., 2016. "Vibration prediction of bladed disks coupled by friction joints". *Archives of Computational Methods in Engineering*, jul.

[14] Gastaldi, C., and Gola, M., 2016. "On the relevance of a microslip contact model for under-platform dampers". *International Journal of Mechanical Sciences,* ***115-116***, pp. 145–156.

[15] Brake, M., 2018. *The Mechanics of Jointed Structures*. Springer, ch. An Overview of Constitutive Models, pp. 207–222.

[16] Xu, C., Li, D., Gola, M. M., and Gastaldi, C., 2018. "A comparison of two microslip contact models for studying the mechanics of underplatform dampers". In Volume 7C: Structures and Dynamics, ASME.

[17] Pesaresi, L., Armand, J., Schwingshackl, C., Salles, L., and Wong, C., 2018. "An advanced underplatform damper modelling approach based on a microslip contact model". *Journal of Sound and Vibration,* ***436***, dec, pp. 327–340.

[18] Yang, B., and Menq, C., 1998. "Characterization of 3d contact kinematics and prediction of resonant response of structures having 3d frictional constraint.". *J Sound Vib,* ***217***(5), p. 90925.

[19] Afzal, M., Arteaga, I. L., and Kari, L., 2016. "An analytical calculation of the jacobian matrix for 3d friction contact model applied to turbine blade shroud contact". *Computers & Structures,* ***177***, dec, pp. 204–217.

[20] Hartung, A., Hackenberg, H.-P., Krack, M., Gross, J., Heinze, T., and von Scheidt, L. P., 2018. "Rig and engine validation of the non-linear forced response analysis performed by the tool OrAgL". In Volume 7C: Structures and Dynamics, ASME.

[21] Gastaldi, C., and Gola, M. M., 2016. "Testing, simulating and understanding under-platform damper dynamics". In Proceedings of the VII European Congress on Computational Methods in Applied Sciences and Engineering (ECCOMAS Congress 2016).

[22] Pesaresi, L., Salles, L., Jones, A., Green, J., and Schwingshackl, C., 2017. "Modelling the nonlinear behaviour of an underplatform damper test rig for turbine applications". *Mechanical Systems and Signal Processing,* ***85***, feb, pp. 662–679.

[23] Gastaldi, C., Berruti, T. M., and Gola, M. M., 2019. "A novel test rig for friction parameters measurement on underplatform dampers". *International Journal of Solids and Structures*, aug.

[24] Gola, M., and Liu, T., 2014. "A direct experimental-numerical method for investigations of a laboratory under-platform damper behavior". *International Journal of Solids and Structures,* ***51***(25-26), pp. 4245–4259.

[25] Gastaldi C., Berruti T.M., G. M. B. A., 2019. "Experimental investigation on real under-platform dampers: the impact of design and manufacturing". In Proceedings of ASME Turbo EXPO 2019.

[26] Fantetti, A., Tamatam, L., Volvert, M., Lawal, I., Liu, L., Salles, L., Brake, M., Schwingshackl, C., and Nowell, D., 2019. "The impact of fretting wear on structural dynamics: Experiment and simulation". *Tribology International,* ***138***, oct, pp. 111–124.

[27] Gastaldi, C., 2017. "Vibration control and mitigation in turbomachinery, phd thesis".

[28] Harris, T. ., and Kotzalas, M., ISBN: 0849381673, 2006. *Rolling Bearing Analysis*, 5th ed. CRC Press.

[29] and, 2018. "Competitive time marching solution methods for systems with friction-induced nonlinearities". *Applied Sciences,* ***8***(2), feb, p. 291.

[30] Craig, R. R., and Bampton, M. C. C., 1968. "Coupling of substructures for dynamic analyses". *AIAA Journal,* ***6***(7), pp. 1313–1319.

[31] Gastaldi, C., and Berruti, T. M., 2017. "A method to solve the efficiency-accuracy trade-off of multi-harmonic balance calculation of structures with friction contacts". *International Journal of Non-Linear Mechanics,* ***92***, jun, pp. 25–40.

[32] Gastaldi, C., and Gola, M. M., 2018. "Criteria for best performance of pre-optimized solid dampers". In ASME Turbo Expo 2018 Volume 7C: Structures and Dynamics, ASME.

List of Figure captions

1. a. View of the Piezo Damper Rig II. b. Close up on one of the platform inserts.
2. Schematic showing how the absolute platform kinematics (left) in case of In Phase blade motion is transformed into relative platform kinematics (middle) and finally simulated changing the test rig configuration (right).
3. a. Relevant quantities of the platform-to-platform hysteresis cycle. b. Observed (dotted line) and simulated (solid line) platform-to-platform hysteresis cycle for Sample 1 at CF=4.65 kg. c. Schematic of measured and reconstructed contact forces. d. Relevant quantities of the platform-to-damper hysteresis cycle. e. Observed (dotted line) and simulated (solid line) platform-to-damper flat-on-flat interface hysteresis cycle for Sample 1 at CF=4.65 kg. f. Tangential over normal force ratios at both interfaces vs. time. Dotted lines: observed, solid lines: simulated.
4. a. Observed (dotted line) and simulated (solid line)contact forces diagram for Sample 1 at CF=4.65 kg. b Representative scheme of the assumed distribution of normal contact springs. c Derived position of the normal component of the left contact force resultant N_L and resulting $q(x)$ at stage 2 of the cycle. d Observed (dotted line) and simulated (solid line) moment vs. rotation diagram for Sample 1 at CF=4.65 kg.
5. a. Schematic of the standard numerical model used to simulate Sample 1 and Sample 5. b. Repeatability of the damper profile for Sample 1. c. Damper vs. platform profiles from Sample 1.
6. a. Observed contact forces diagram for Sample 2 at CF=4.65 kg. b. Observed movement vs rotation diagram for Sample 2 at CF=4.65 kg. c. Damper vs. platform profiles for Sample 2.
7. a. Comparison between the measured platform-to-platform hysteresis cycles from Samples 1 and 2 at CF= 4.65 kg. b. Corresponding platform-to-damper hysteresis cycle for Sample 2.
8. Comparison between platform-to-platform hysteresis cycles: Samples 3 to 5 at 250Hz and CF= 10 kg.
9. Profilometer scan for the platform insert of Sample 3.
10. a. Contact forces diagram and b. rotation signal measured on Sample 3 at 250 Hz and CF=10 kg.
11. a. Platform-damper profile b. Contact forces diagram and c. rotation signal for a 250 Hz CF=10 kg measured on Sample 4
12. a. Contact forces diagram and b. rotation signal for a 250 Hz CF=10 kg measured on Sample 5
13. a. Comparison between simulated platform-to-platform hysteresis cycles for Samples 3 to 5. Their measured counterpart can be found in Fig. 8. b.-c. Schematic of the numerical model used to obtain the numerical cycles for Samples 3 and 4 respectively.
14. Schematic of FRIDA, the in-house nonlinear solver for the prediction of the dynamic response of bladed disks. The right portion of the scheme shows a forced response result comparison for Samples 3 to 5.

Journal of Vibration and Acoustics. Received August 19, 2019;
Accepted manuscript posted January 17, 2020. doi:10.1115/1.4046954

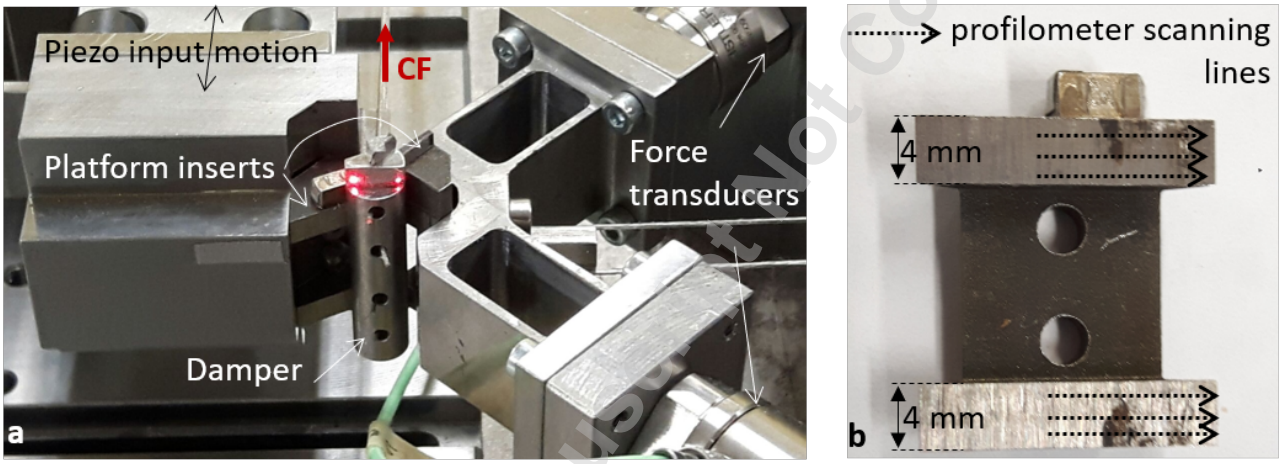

Fig. 1. a. View of the Piezo Damper Rig II. b. Close up on one of the platform inserts.

Journal of Vibration and Acoustics. Received August 19, 2019;
Accepted manuscript posted January 17, 2020. doi:10.1115/1.4046954

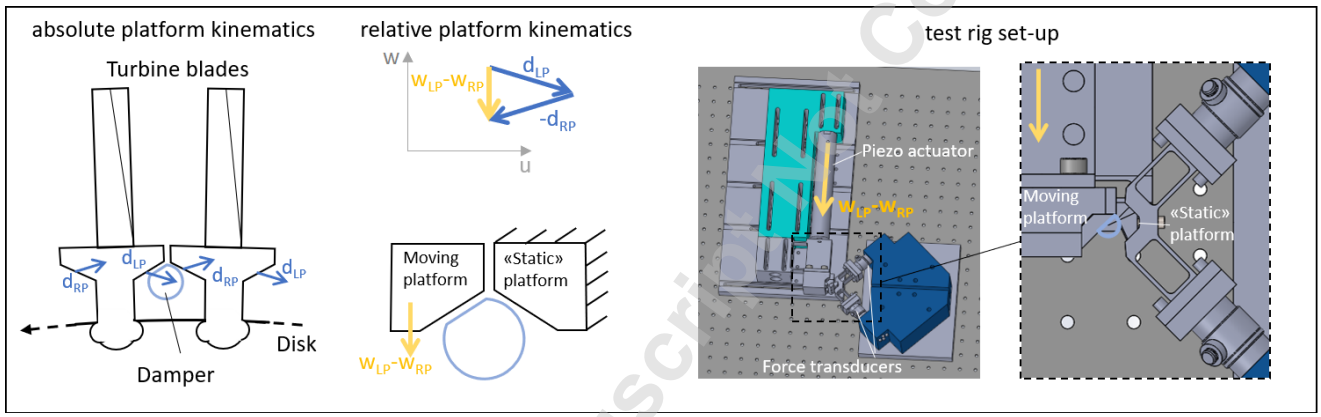

Fig. 2. Schematic showing how the absolute platform kinematics (left) in case of In Phase blade motion is transformed into relative platform kinematics (middle) and finally simulated changing the test rig configuration (right).

Journal of Vibration and Acoustics. Received August 19, 2019;
Accepted manuscript posted January 17, 2020. doi:10.1115/1.4046954

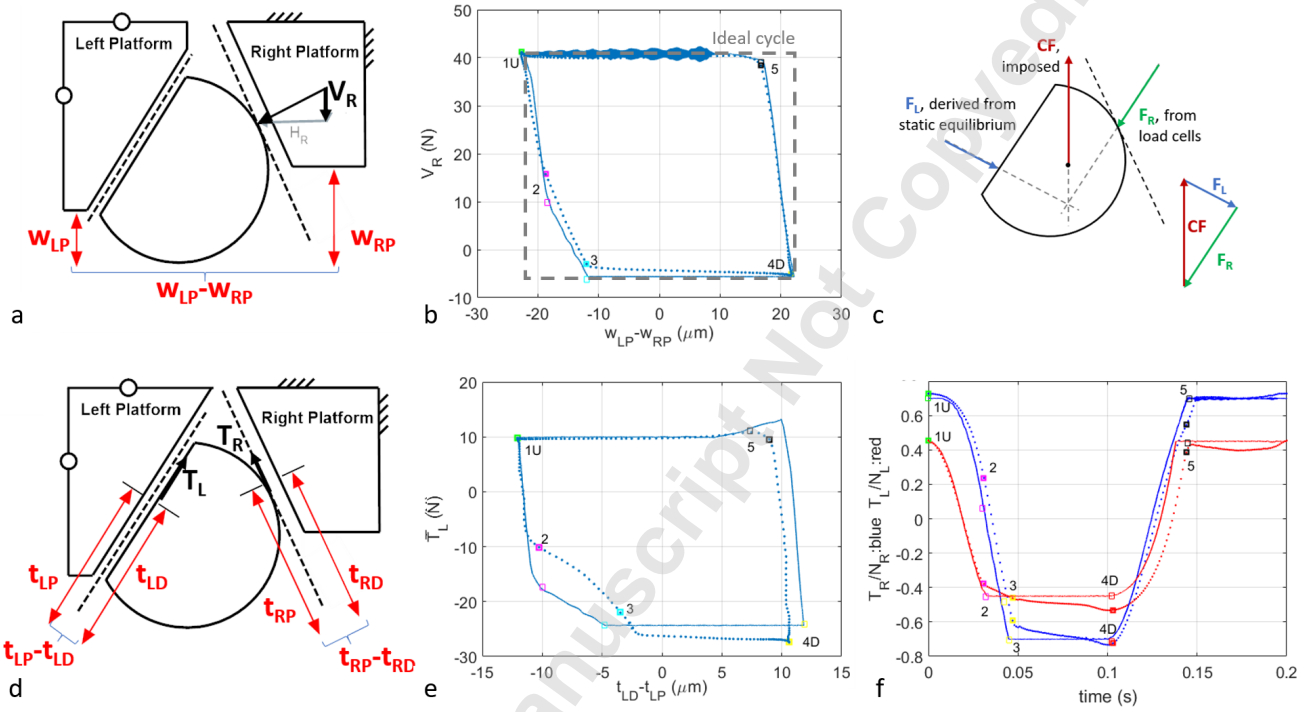

Fig. 3. a. Relevant quantities of the platform-to-platform hysteresis cycle. b. Observed (dotted line) and simulated (solid line) platform-to-platform hysteresis cycle for Sample 1 at CF=4.65 kg. c. Schematic of measured and reconstructed contact forces. d. Relevant quantities of the platform-to-damper hysteresis cycle. e. Observed (dotted line) and simulated (solid line) platform-to-damper flat-on-flat interface hysteresis cycle for Sample 1 at CF=4.65 kg. f. Tangential over normal force ratios at both interfaces vs. time. Dotted lines: observed, solid lines: simulated.

Journal of Vibration and Acoustics. Received August 19, 2019;
Accepted manuscript posted January 17, 2020. doi:10.1115/1.4046954

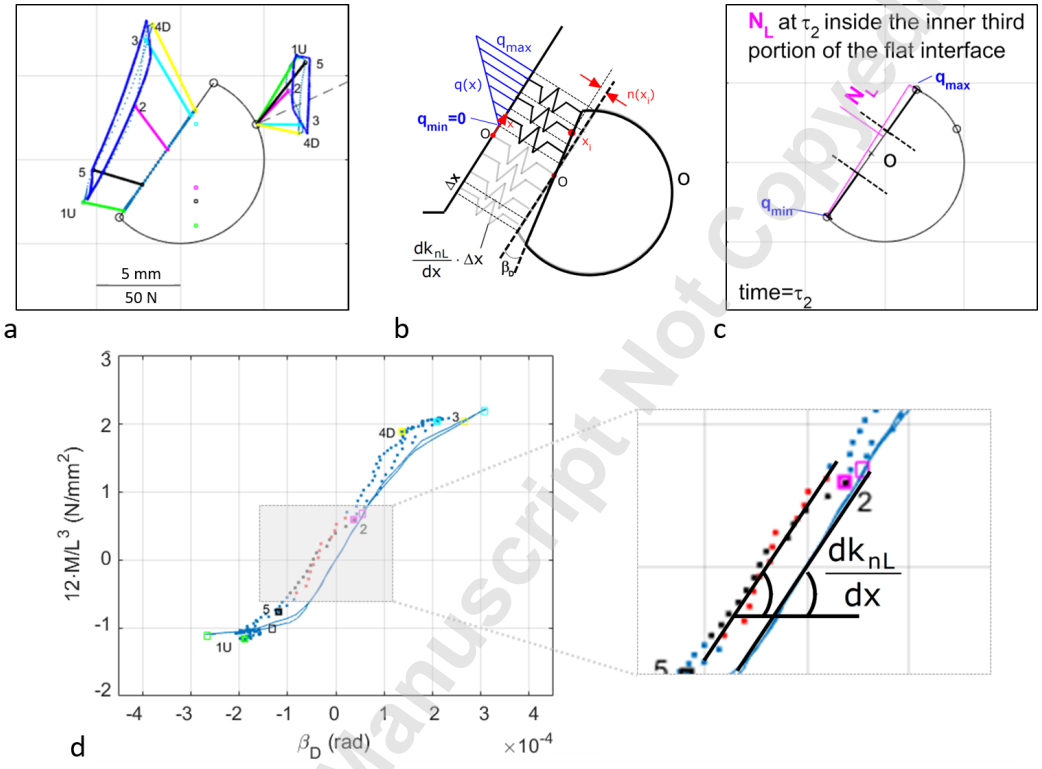

Fig. 4. a Observed (dotted line) and simulated (solid line)contact forces diagram for Sample 1 at CF=4.65 kg. b Representative scheme of the assumed distribution of normal contact springs. c Derived position of the normal component of the left contact force resultant N_L and resulting $q(x)$ at stage 2 of the cycle. d Observed (dotted line) and simulated (solid line) moment vs. rotation diagram for Sample 1 at CF=4.65 kg.

Journal of Vibration and Acoustics. Received August 19, 2019;
Accepted manuscript posted January 17, 2020. doi:10.1115/1.4046954

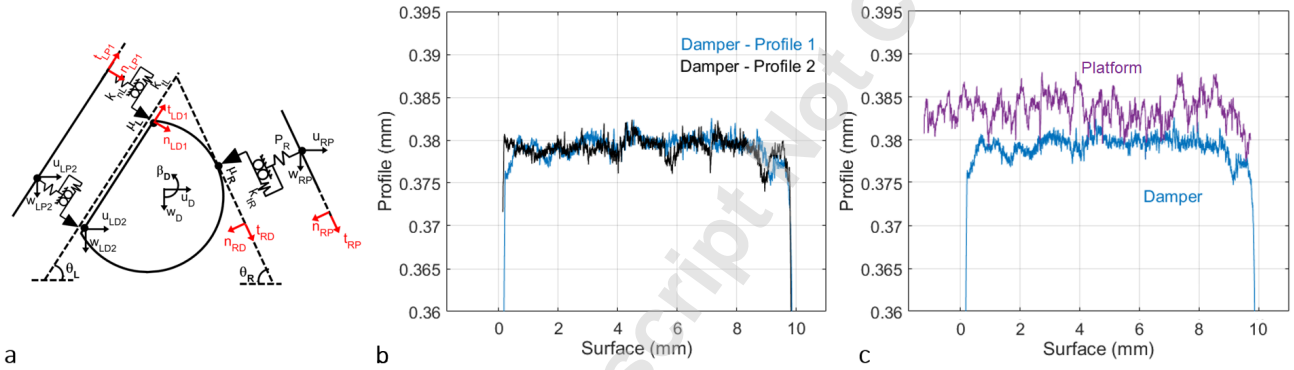

Fig. 5. a. Schematic of the standard numerical model used to simulate Sample 1 and Sample 5. b. Repeatability of the damper profile for Sample 1. c. Damper vs. platform profiles from Sample 1.

Journal of Vibration and Acoustics. Received August 19, 2019;
Accepted manuscript posted January 17, 2020. doi:10.1115/1.4046954

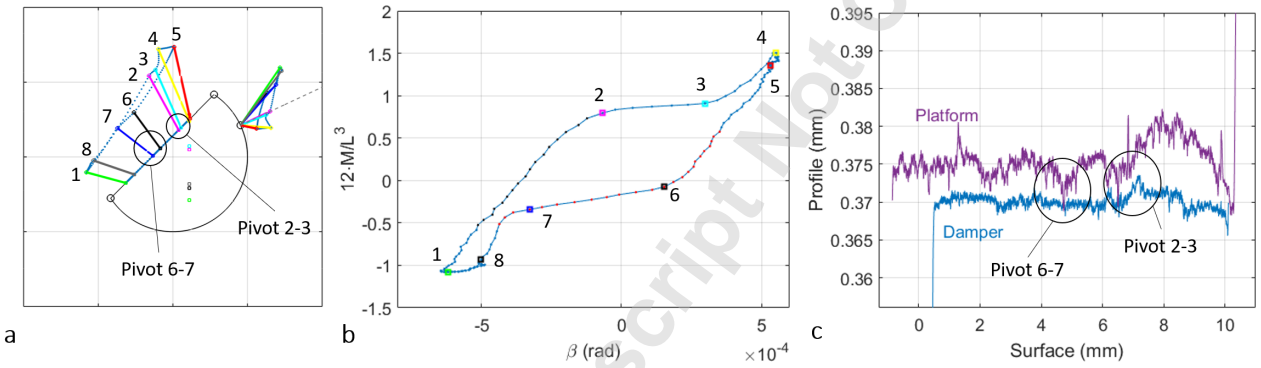

Fig. 6. a. Observed contact forces diagram for Sample 2 at CF=4.65 kg. b. Observed movement vs rotation diagram for Sample 2 at CF=4.65 kg. c. Damper vs. platform profiles for Sample 2.

Journal of Vibration and Acoustics. Received August 19, 2019;
Accepted manuscript posted January 17, 2020. doi:10.1115/1.4046954

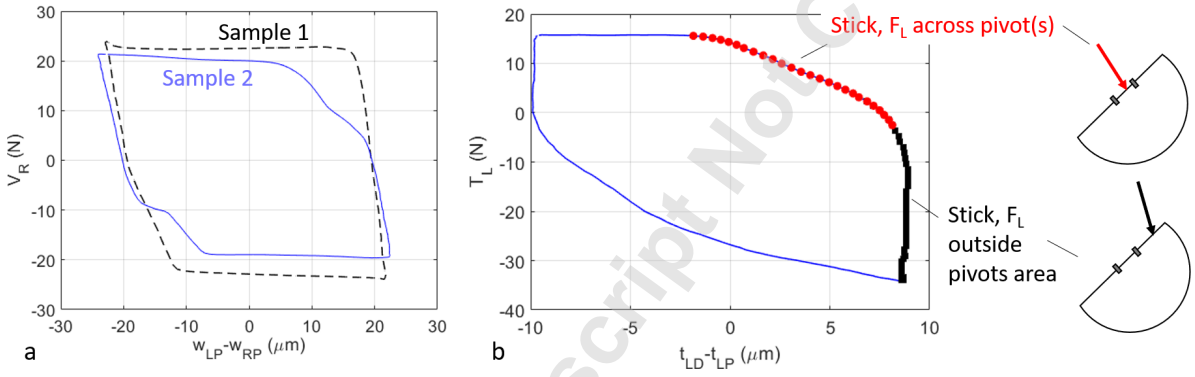

Fig. 7. a. Comparison between the measured platform-to-platform hysteresis cycles from Samples 1 and 2 at CF= 4.65 kg. b. Corresponding platform-to-damper hysteresis cycle for Sample 2.

Journal of Vibration and Acoustics. Received August 19, 2019;
Accepted manuscript posted January 17, 2020. doi:10.1115/1.4046954

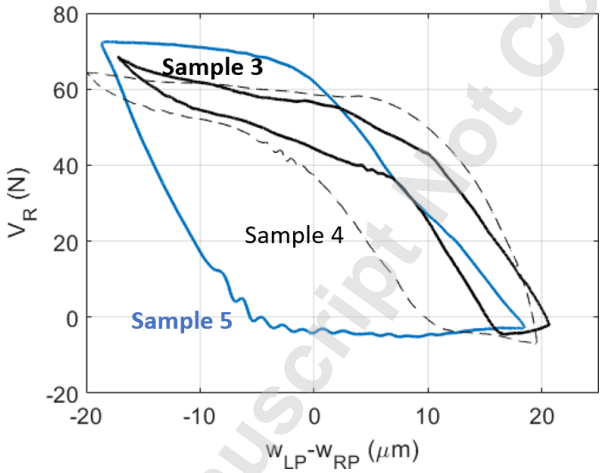

Fig. 8. Comparison between platform-to-platform hysteresis cycles: Samples 3 to 5 at 250Hz and CF= 10 kg.

Journal of Vibration and Acoustics. Received August 19, 2019;
Accepted manuscript posted January 17, 2020. doi:10.1115/1.4046954

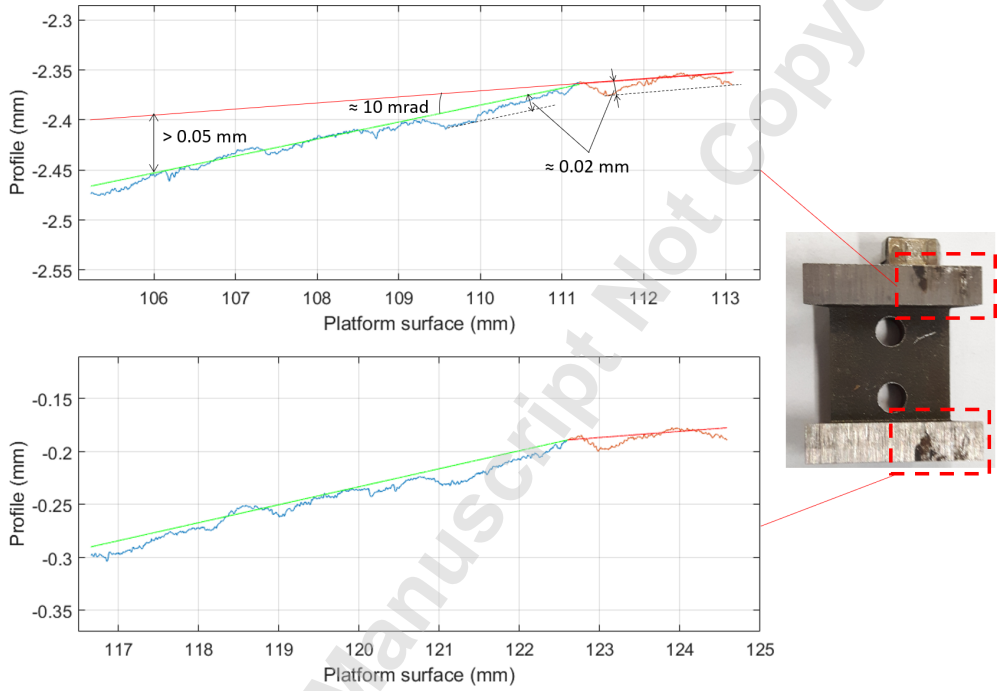

Fig. 9. Profilometer scan for the platform insert of Sample 3.

Journal of Vibration and Acoustics. Received August 19, 2019;
Accepted manuscript posted January 17, 2020. doi:10.1115/1.4046954

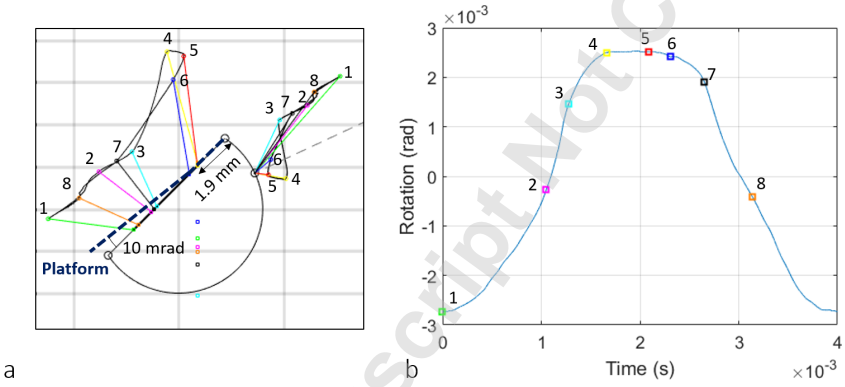

Fig. 10. a. Contact forces diagram and b. rotation signal measured on Sample 3 at 250 Hz and CF=10 kg.

Journal of Vibration and Acoustics. Received August 19, 2019;
Accepted manuscript posted January 17, 2020. doi:10.1115/1.4046954

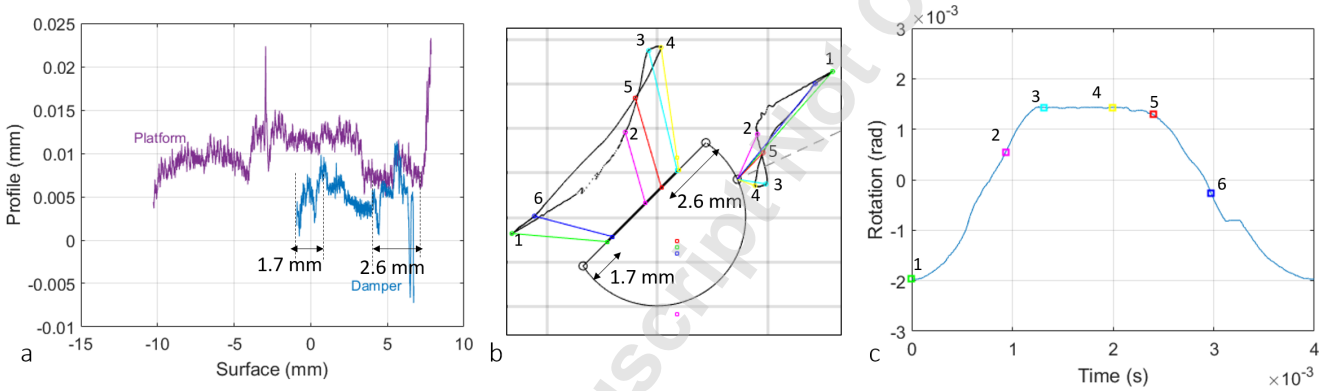

Fig. 11. a. Platform-damper profile b. Contact forces diagram and c. rotation signal for a 250 Hz CF=10 kg measured on Sample 4

Journal of Vibration and Acoustics. Received August 19, 2019;
Accepted manuscript posted January 17, 2020. doi:10.1115/1.4046954

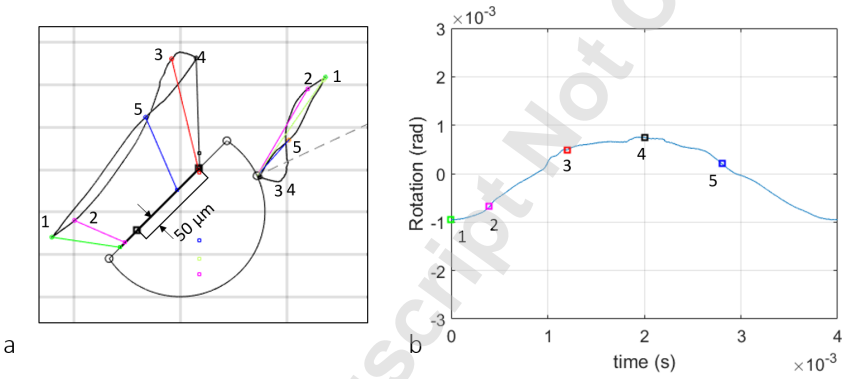

Fig. 12. a. Contact forces diagram and b. rotation signal for a 250 Hz CF=10 kg measured on Sample 5

Journal of Vibration and Acoustics. Received August 19, 2019;
Accepted manuscript posted January 17, 2020. doi:10.1115/1.4046954

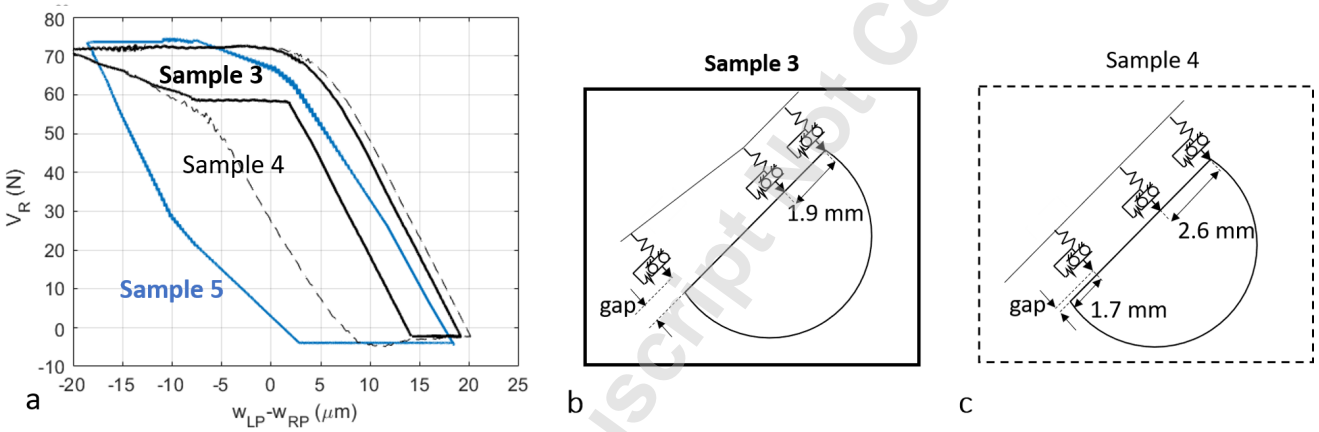

Fig. 13. a. Comparison between simulated platform-to-platform hysteresis cycles for Samples 3 to 5. Their measured counterpart can be found in Fig. 8. b.-c. Schematic of the numerical model used to obtain the numerical cycles for Samples 3 and 4 respectively.

Journal of Vibration and Acoustics. Received August 19, 2019;
Accepted manuscript posted January 17, 2020. doi:10.1115/1.4046954

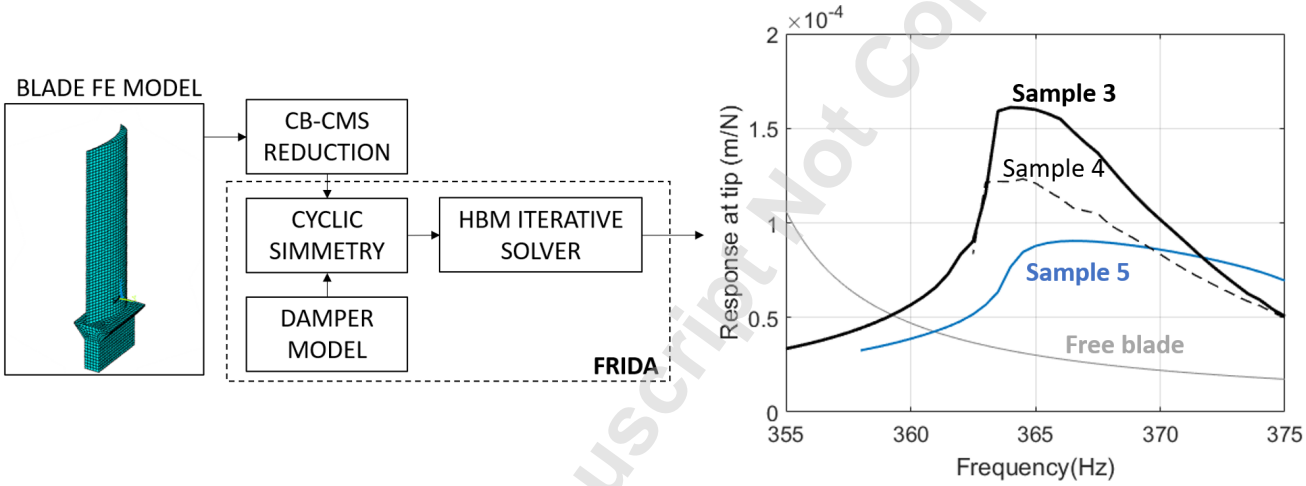

Fig. 14. Schematic of FRIDA, the in-house nonlinear solver for the prediction of the dynamic response of bladed disks. The right portion of the scheme shows a forced response result comparison for Samples 3 to 5.

Journal of Vibration and Acoustics. Received August 19, 2019;
Accepted manuscript posted January 17, 2020. doi:10.1115/1.4046954

List of Table captions

Table 1. Main characteristics of the five damper-platform samples tested within this work

Journal of Vibration and Acoustics. Received August 19, 2019;
Accepted manuscript posted January 17, 2020. doi:10.1115/1.4046954

Table 1. Main characteristics of the five damper-platform samples tested within this work

Sample id.	Material	Rig	Centrifugal load (kg)	Frequency range	Damping efficiency (%)
1	Steel	Piezo Rig I	2-8	<80 Hz	80
2	Steel	Piezo Rig I	2-8	<80 Hz	71
3	Rene' 80	Piezo Rig II	10-30	<300 Hz	16
4	Rene' 80	Piezo Rig II	10-30	<300 Hz	32
5	Rene' 80	Piezo Rig II	10-30	<300 Hz	57